ARTICLE NO. 78-1255R

# High-Accuracy Calibration of Electrostatic Gyro Strapdown Navigation Systems

R.L. Blanchard*
*Rockwell International, Anaheim, Calif.*

**A one-half order of magnitude accuracy improvement is obtained for an electrostatic gyro strapdown navigation system using a high-accuracy calibration technique. The system achieves cancellation of instrument errors by rotating the instrument cluster. The instrument errors that do not cancel out with rotation are modeled in a rotated function space. The coefficients of the rotated function space are obtained with a calibration that uses Kalman filtering. These are used to update the instrument model coefficients in a nonrotated function space. Flight test results are presented that show navigation accuracy with and without a high-accuracy calibration.**

## Introduction

An electrostatic gyro (ESG) is characterized by extremely low random drift rates and a complex error model. The accuracy of a navigation system containing an ESG is limited by how well it can be calibrated. This paper shows how a one-half order of magnitude accuracy improvement has been obtained, using a high accuracy calibration technique, for an ESG strapdown navigation system that rotates the instrument assembly unit (IAU) about an axis nominally colinear with the vehicle yaw axis. The system is the N73 Strapdown Navigator developed by Rockwell International.

Rotating the IAU causes the ESG error sources to either cancel out or be attenuated. The high accuracy calibration is performed at the system level with the IAU rotating. Hence, only error sources that do not cancel out with rotation are seen by the high-accuracy calibration. The error sources that do not cancel out with rotation are modeled in a coordinate system in which only average effects are seen during one rotation period. This model is referred to as the rotated function space.

The coefficients of the rotated function space are used to update the coefficients of the nonrotated ESG model. Because of this, the navigation computer requires no additional software.

## Description of System

The heart of the N73 Strapdown Navigation System is the ESG. An exploded isometric drawing of its constituent parts is presented in Fig. 1. The rotor is a solid 1-cm beryllium ball weighing 1 g. The rotor is supported in a cavity (shown in Fig. 2) consisting of eight plates which are also used to sense its spin-axis orientation. The rotor is intentionally given a radial mass unbalance by the insertion of three tantalum wires. The mass unbalance is required for sensing the spin-axis orientation. The ESG has a whole-angle readout capability which eliminates the necessity of extrapolating the vehicle direction cosines. A thorough description of the ESG is presented in the literature.[1]

The N73 electromagnetic accelerometer (EMA) is a single-axis, force rebalance inertial sensor whose microminiaturized restoration servo and digitizer electronics are self contained. The EMA is described in more detail in the literature.[2]

The N73 strapdown navigator consists of the instrument assembly unit (IAU) shown in Fig. 3, the computer, and the associated electronics. The IAU contains three EMA's and two ESG's. Each ESG provides two sensing axes. The ESG's (whose cases are mounted identically) are spun up with their spin axes orthogonal. One sensing axis of one of the ESG's is numerically caged to one sensing axis of the other ESG. The IAU is rotated at 1 rpm about an axis nominally conlinear with the vehicle yaw axis. The direction of rotation reverses every 360 deg. Hence, the rotation period is two minutes. Because the navigator is a strapdown system, the only effect

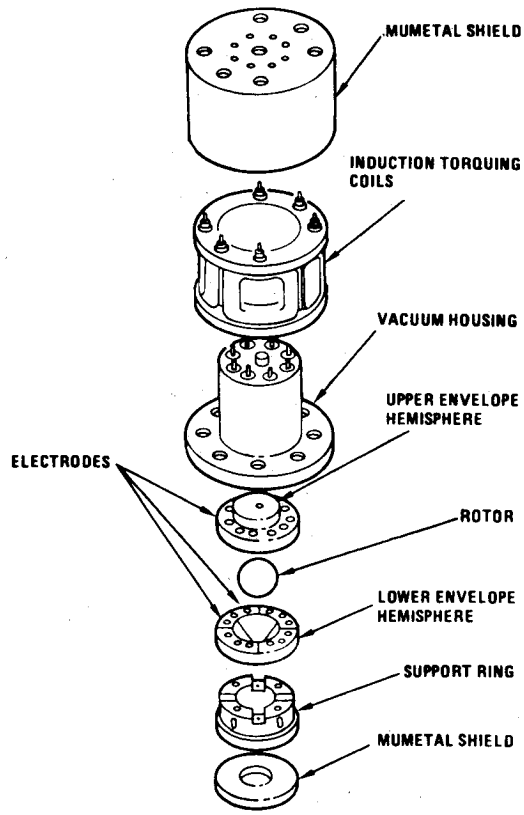


**Fig. 1 MESG exploded view.**

Presented as Paper 78-1255 at the AIAA Guidance and Control Conference, Palo Alto, Calif., Aug. 7-9, 1978; submitted Sept. 19, 1978; revision received Feb. 14, 1979. 

Index category: Guidance and Control.

*Member of Technical Staff, Strapdown Navigation Systems, Autonetics Strategic Systems Division

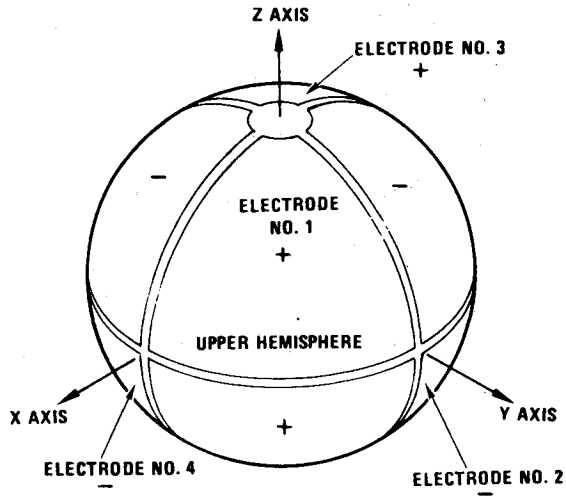


Fig. 2 ESG cavity configuration.

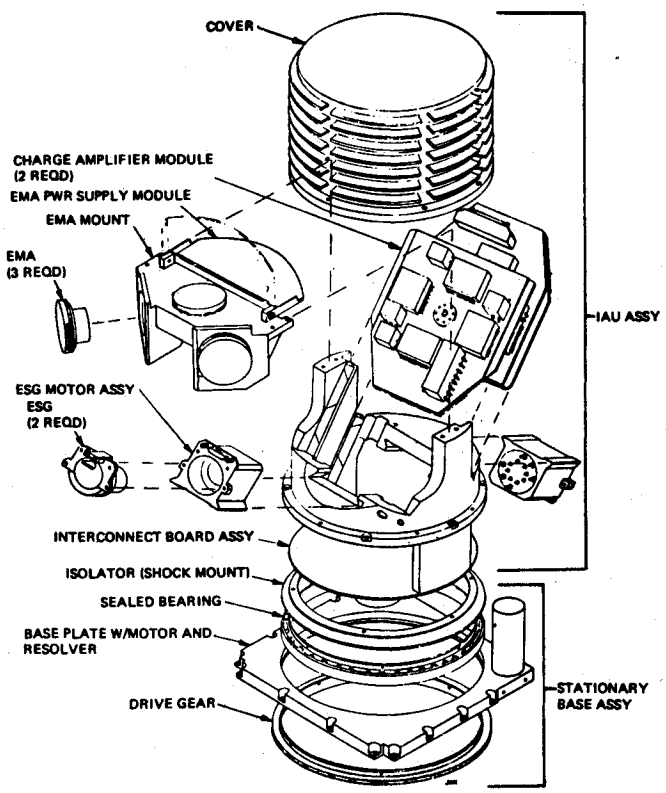


Fig. 3 N73 instrument assembly unit (IAU).

of the rotation reversal is in the processing of the velocity data. The software synchronizes the rotation reversal with the collection of velocity data.

## Development of Rotated Model

The ESG angle readout and drift rate models are given in a coordinate system fixed with respect to the ESG case. The angle readout model contains 56 terms, none of which are $g$-dependent. It can be represented by spherical harmonics given in terms of latitude and longitude of the spin vector pierce point on a surrounding sphere (see Fig. 4). A physical examination of Fig. 4 shows that if the case is rotated about a vector $\bar{I}_r$ called the rotation axis, average errors will remain about a vector $\bar{I}_t$ (called track) perpendicular to the plane of the spin vector $\bar{\gamma}$ and $\bar{I}_r$, and about a vector $\bar{I}_c$ (called cross-track) which is perpendicular to both $\bar{\gamma}$ and $\bar{I}_t$. The following convention is used for the track and cross-track vectors for

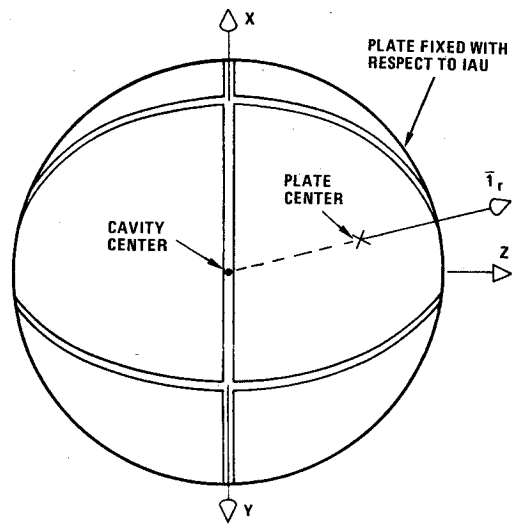


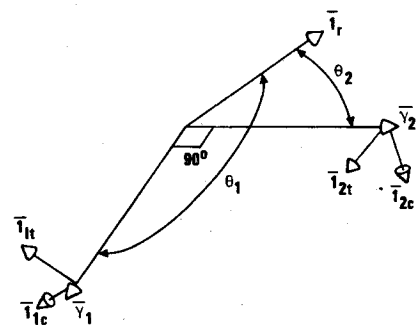


Fig. 4 Rotated error model coordinate geometry.

the $i$th ESG:

$$\bar{I}_{it} = \bar{\gamma}_i \times \bar{I}_r / |\bar{\gamma}_i \times \bar{I}_r| \tag{1}$$

$$\bar{I}_{ic} = \bar{\gamma}_i \times \bar{I}_{it} \tag{2}$$

It can also be seen that when $\bar{\gamma}$ and $\bar{I}_r$ are colinear, the average errors are zero. It can be shown that the average (rotated) angle readout model can be represented by

$$\tilde{\alpha}_i = \left[\sum_{n=1}^{N_\alpha} P_{nit} \sin(n\theta_i)\right] \bar{I}_{it} + \left[\sum_{n=1}^{N_\alpha} P_{nic} \sin(n\theta_i)\right] \bar{I}_{ic} \qquad (i=1,2) \tag{3}$$

where

$$\begin{aligned} \theta_i &= \cos^{-1}(\bar{\gamma}_i \cdot \bar{I}_r) \\ \bar{\gamma}_i &= i\text{th ESG spin vector} \\ \tilde{\alpha}_i &= \text{angle readout error (angular) for } i\text{th ESG} \\ P_{nit}, P_{nic} &= \text{model coefficients} \\ N_\alpha &= \text{degree of polynomial expansion} \end{aligned} \tag{4}$$

The ESG nonrotated angle readout model contains 56 terms. Since the rotated angle readout model is based on the nonrotated angle readout model, a linear transformation matrix $(M_\alpha)$ exists which maps the nonrotated model coefficients onto the rotated model coefficients. The mapping of the nonrotated angle readout model coefficients onto the rotated angle readout model coefficients is given by

$$\begin{bmatrix} P_{it} \\ \hline P_{ic} \end{bmatrix} = [M_\alpha]\,[\Delta\gamma_i] \tag{5}$$

where

$\Delta\gamma_i$ = array of nonrotated angle readout model coefficients for $i$th gyro

The transformation has been determined using numerical integration for $N_\alpha = 25$. The resulting transformation shows that all of the harmonics above the fourth in the rotated model can be neglected. Consequently, $N_\alpha$ has been taken to be 4. This results in $M_\alpha$ being an $8 \times 56$ matrix.

The ESG drift rate model contains 31 non-$g$- and 7$g$-dependent terms. The non-$g$-dependent terms can be represented by spherical harmonics. The average (rotated) drift rate model for non-$g$-dependent terms is obtained by following the same reasoning used to obtain the rotated angle readout model:

$$\bar{\epsilon}_i = \left[\sum_{n=1}^{N_\epsilon} Q_{nit}\sin(n\theta_i)\right]\bar{I}_{it} + \left[\sum_{n=1}^{N_\epsilon} Q_{nic}\sin(n\theta_i)\right]\bar{I}_{ic} \quad (6)$$

where

$\bar{\epsilon}_i$ = drift rate error for $i$th ESG
$Q_{nit}, Q_{nic}$ = model coefficients

The transformation matrix ($M_\epsilon$) which maps the nonrotated drift rate model coefficients onto the rotated drift rate model coefficients is defined by

$$\begin{bmatrix} Q_{it} \\ \hline Q_{ic} \end{bmatrix} = [M_\epsilon]\,[\Delta\epsilon_i] \quad (7)$$

where

$\Delta\epsilon_i$ = array of nonrotated drift rate model coefficients for the $i$th gyro

The $g$-dependent terms in the nonrotated model are numbered 4, 11, 24, 32, 33, 34, and 35. Hence, the columns in $M_\epsilon$ corresponding to these numbers are zero. The rest of the elements in $M_\epsilon$ were determined using numerical integration, as was done for $M_\alpha$. The resulting transformation shows that only harmonics 1 and 2 are significant for track and harmonics 1, 2, and 4 for cross-track. For purposes of validating the model, the fourth harmonic for track has been retained. This results in $M_\epsilon$ being a $6 \times 38$ matrix.

The $g$-dependent drift rate model terms in rotated space are obtained by transforming the nonrotated model terms to the $\bar{I}_{it}$, $\bar{I}_{ic}$, $\bar{\gamma}_i$ coordinate frame and averaging. The resulting rotated drift rate model is of the form

$$\bar{\epsilon}_{gni} = E_{ni}\left\{\left[\sum_{l,j,k,m} A_{tniljkm} a_t^l a_c^j a_\gamma^k \mathrm{trig}(m\theta_i)\right]\bar{I}_{it} + \left[\sum_{l,j,k,m} A_{cniljkm} a_t^l a_c^j a_\gamma^k \mathrm{trig}(m\theta_i)\right]\bar{I}_{ic}\right\} \quad (8)$$

where

$\bar{\epsilon}_{gni}$ = rotated drift rate error for the $n$th $g$-sensitive drift rate term of the $i$th ESG
$E_{ni}$ = rotated $g$-sensitive drift rate coefficient for $n$th term of the $i$th ESG
$A$ = model coefficient
$a$ = sensed acceleration
$t$ = track component
$c$ = cross-track component
$\gamma$ = spin axis component
$\mathrm{trig}(m\theta_i) = \begin{cases} \sin(m\theta), & \text{if } m > 0 \\ \cos(m\theta), & \text{if } m \le 0 \end{cases}$

This model form has been demonstrated using closed-form solutions. It contains a total of 28 terms. The coefficient matrix ($A$) was determined for the entire model by generating combinations of conditions and performing a least-squares fit.

The mapping of the nonrotated $g$-sensitive drift rate coefficients onto the rotated $g$-sensitive coefficients is one-to-one with a reordering. It is given by

$$[E_{ni}] = [M_{\epsilon g}]\,[\Delta\epsilon_i] \quad (9)$$

The transformation matrix ($M_{\epsilon g}$) is a $7 \times 38$ which contains one's for elements (1,4), (2,11), (3,24), (4,32), (5,33), (6,34), and (7,35), and zero's for the rest of the elements. Combining Eqs. (7) and (9) we have

$$\begin{bmatrix} Q_{it} \\ \hline Q_{ic} \\ \hline E_i \end{bmatrix} = \begin{bmatrix} M_\epsilon \\ \hline M_{\epsilon g} \end{bmatrix} [\Delta\epsilon_i] \quad (10)$$

## Propagation of Rotated Model into System Velocity Errors

The crux of the high-accuracy rotated calibration scheme is the determination of the coefficients of the rotated model function space. The coefficients are obtained by processing velocity measurements taken for various system orientations while the system is operating in the navigation mode with the Schuler loops opened and the IAU rotating. Coefficients from a nonrotated calibration have already been entered into the navigation computer. The processing requires the propagation of the rotated angle readout and drift rate models into system velocity errors.

Angle readout errors propagate directly into system velocity errors. The propagation is obtained by substituting Eq. (3) for angle readout error into Eq. (11) (obtained from Ref. 3). This equation models the propagation of angle readout errors into system velocity errors. It takes into account the fact that two 2-degree-of-freedom ESG's are used as the inertial reference, with the redundant axis of the number-two ESG numerically caged to the number-one ESG.

$$\frac{\mathrm{d}}{\mathrm{d}t}\Delta\bar{V} = T_{sn} \times \left\{ \begin{bmatrix} \bar{A}^T \\ (1/S)\left[-(1+C^2)\bar{A}\cdot\bar{\gamma}_1 + C\bar{A}\cdot\bar{\gamma}_2\right]\bar{\gamma}_2^T - (C/S)\bar{A}^T \\ (1/S(\bar{\gamma}_2\times\bar{A})^T + (C/S)\bar{A}\cdot(\bar{\gamma}_1\times\bar{\gamma}_2)\bar{\gamma}_2^T \end{bmatrix} \Delta\bar{\gamma}_1 + \begin{bmatrix} 0 \\ (1/S)\left[-(1+C^2)\bar{A}\cdot\bar{\gamma}_1 + C\bar{A}\cdot\bar{\gamma}_2\right]\bar{\gamma}_1^T + (1/S)\bar{A}^T \\ (1/S)(\bar{A}\times\bar{\gamma}_1)^T + (C/S)\bar{A}\cdot(\bar{\gamma}_1\times\bar{\gamma}_2)\bar{\gamma}_1^T \end{bmatrix} \Delta\bar{\gamma}_2 \right\} \quad (11)$$

where

$T_{sn}$ = transformation matrix from spin to navigation coordinates (east, north, up)
$\Delta\bar{\gamma}_i$ = angle readout error (displacement) of $i$th ESG
$\bar{A}$ = acceleration vector
$C$ = $\bar{\gamma}_1\cdot\bar{\gamma}_2$
$S$ = $(1-C^2)^{1/2}$

Substituting $\Delta\bar{\gamma}_i = \bar{\alpha}_i \times \bar{\gamma}_i$ into Eq. (11) we have

$$\frac{d}{dt}\Delta\bar{V} = T_{sn} \times \left\{ \begin{bmatrix} \bar{A}^T \\ (1/S)\left[-(1+C^2)\bar{A}\cdot\bar{\gamma}_1 + C\bar{A}\cdot\bar{\gamma}_2\right]\bar{\gamma}_2^T - (C/S)\bar{A}^T \\ (1/S(\bar{\gamma}_2\times\bar{A})^T + (C/S)\bar{A}\cdot(\bar{\gamma}_1\times\bar{\gamma}_2)\bar{\gamma}_2^T \end{bmatrix} \left\{ \left[\sum_{n=1}^{N} P_{nlt}\sin(n\theta_1)\right]\bar{I}_{1t} + \left[\sum_{n=1}^{N} P_{nlc}\sin(n\theta_1)\right]\bar{I}_{1c} \right\} \times \bar{\gamma}_1 \right.$$

$$\left. + \begin{bmatrix} 0 \\ (1/S)\left[-(1+C^2)\bar{A}\bar{\gamma}_1 + C\bar{A}\cdot\bar{\gamma}_2\right]\bar{\gamma}_1^T + (I/S)\bar{A}^T \\ (1/S)(\bar{A}\times\bar{\gamma}_1)^T + (C/S)\bar{A}\cdot(\bar{\gamma}_1\times\bar{\gamma}_2)\bar{e}_1^T \end{bmatrix} \left\{ \left[\sum_{n=1}^{N} P_{n2t}\sin(n\theta_2)\right]\bar{I}_{2t} + \left[\sum_{n=1}^{N} P_{n2c}\sin(n\theta_2)\right]\bar{I}_{2c} \right\} \times \bar{\gamma}_2 \right\} \quad (12)$$

Drift rate errors propagate into system velocity errors through system misalignments. The propagation of ESG drift rate errors into system misalignment is given by[3]

$$\frac{d}{dt}\bar{\varphi} = -\frac{I}{S^2}\left[\{\bar{\gamma}_1\cdot(\bar{\epsilon}_2+\bar{\epsilon}_{g2})\}\bar{\gamma}_1 + \{\bar{\gamma}_2\cdot(\bar{\epsilon}_1+\bar{\epsilon}_{g1})\}\bar{\gamma}_2\right] - \{\bar{\gamma}_3\cdot(\bar{\epsilon}_1+\bar{\epsilon}_{g1})\} \quad (13)$$

where

$\bar{\varphi}$ = misalignment vector in inertial space
$\bar{\gamma}_3 = (1/\Lambda)\bar{\gamma}_1 \times \bar{\gamma}_2$

Equation (13) takes into account the redundant axis caging of the number-2 ESG. The propagation of the misalignment vector into system velocity errors is given by

$$d/dt\Delta\bar{V} = T_{sn}\bar{\varphi}\times A \quad (14)$$

Since system velocity errors are used as the measurement for the high-accuracy calibration, electromagnetic accelerometer (EMA) errors which propagate into velocity errors must be modeled. The modeled EMA errors that do not cancel out with rotation are Z-EMA bias ($\Delta A_{zb}$), Z-EMA scale factor ($\Delta A_{zsf}$), and a composite X, Y-EMA scale factor error ($\Delta A_{xysf}$). The propagation of these EMA errors into velocity errors is given by

$$\frac{d}{dt}\Delta\bar{V} = T_{sn}\left[\Delta A_{zb}\bar{I}_r + \Delta A_{zsf}(\bar{A}\cdot\bar{I}_r)\bar{I}_r + \Delta A_{xysf}\bar{I}_r\times(\bar{A}\times\bar{I}_r)\right] \quad (15)$$

The propagation of the rotated model into system velocity errors can be described using state space notation. The state vector $X$ which contains 51 states is defined by

$$X = \begin{bmatrix} \Delta\bar{V} \\ \bar{\varphi} \\ \Delta A_{zb} \\ \Delta A_{zsf} \\ \Delta A_{xysf} \\ P_{1t} \\ P_{1c} \\ P_{2t} \\ P_{2c} \\ Q_{1t} \\ Q_{1c} \\ E_1 \\ Q_{2t} \\ Q_{2c} \\ E_2 \end{bmatrix} \begin{matrix} 3 \\ 3 \\ 1 \\ 1 \\ 1 \\ 4 \\ 4 \\ 4 \\ 4 \\ 3 \\ 3 \\ 7 \\ 3 \\ 3 \\ 7 \end{matrix} \quad (16)$$

The plant is an inertial system in which the Schuler loops have been opened. The system description matrix for the plant is given by Eqs. (12) through (15).

## Calibration Programs

The high-accuracy calibration is performed with the N73 mounted on a Goerz table. The table is sequentially positioned under computer control to provide various orientations of the IAU rotation axis with respect to the ESG spin axes so that observability is obtained. System velocity measurements are recorded for several back and forth rotation periods at each orientation. Velocity is initialized to zero at the beginning of the first rotation period for each orientation and is summed for the remaining rotation periods. The velocity measurements are processed with a computer program to obtain estimates of the rotated model coefficients. At the time the high-accuracy calibration is performed, a nonrotated calibration has already been performed and the coefficients have been entered into the navigation computer.

The high-accuracy calibration software is segmented into three programs. These programs perform the following functions: 1) table control and data collection, 2) rotated model coefficients estimation, and 3) update nonrotated model coefficients with rotated model coefficients.

The Table Control and Data Collection Program controls the three-axis automatic calibration table (Goerz) and samples N73 system data via a serial link between the test-station computer and the N73 navigation computer. The test-station computer is a Hewlett Packard 2100. Input to the program specifies the table orientations and the number of rotation periods at each orientation. The first orientation is with the rotation axis polar and is referred to as a closure point. This orientation is repeated several times in the sequence of orientations to help uncorrelate the ESG angle readout and drift rate models. The next three orientations are with the rotation axis up, down, and north, respectively. These serve to calibrate the EMA error model. This is followed by a series of sweeps of the rotation axis in the three planes defined by the two ESG spin axes and their cross product. At the end of each sweep, the closure point is returned to. The final orientation is with the rotation axis vertical. The purpose of this orientation is to obtain a preferential calibration weighted in favor of the geometry which is present during alignment and early navigation. A total of 51 orientations, each with 8 rotation periods of 2 min each, are used for the high-accuracy calibration. The program outputs at the end of each rotation period are time, system velocity error, and the direction cosines of the rotation axis and ESG spin axes in navigation coordinates.

The rotated model coefficients estimation program uses Carlson's square-root version of the Kalman filter[4] to obtain the rotated model coefficients estimate. The Choe-Tapley

method[5] is used to propagate the state error covariance matrix. A root-sum-square (rss) technique is used to add process noise to the state error covariance matrix. The state error vector for the filter is given by Eq. (16). The direction cosines of the rotation axis and ESG spin axes are used to compute the system description matrix given by Eqs. (12-15).

The rotated model coefficients estimation program also has the capability of computing and plotting the angle readout and drift rate residual estimation errors for each orientation. This is accomplished using a combination of smoothing and least-squares curve-fitting. After the filter pass is performed on the velocity measurements, a backwards smoothing pass is performed using the Rauch Tung-Striebel optimal smoothing technique.[6] The angle readout and drift rate states are nondynamic. Hence, the final Kalman estimate for these states is the same as the smoothed estimate. The smoothing pass provides smoothed estimates of the velocity, misalignment, and accelerometer error states. For each orientation, the smoothed state vector is extrapolated backward using the system description matrix from the end of the first rotation period to the beginning of the first rotation period. Velocity is reinitialized to zero and the state estimate is extrapolated forward for the number of rotation periods at that orientation. This yields corrected velocity estimates for each rotation period. Residual velocity errors are computed by taking the differences between the measured velocities and corrected velocities. A least-squares curve fit is performed on the residual velocity errors for each orientation to obtain residual angle readout and drift rate errors. Figure 5 presents an example of the measured, corrected, and residual velocities, for one orientation.

Programming the rotated model on the navigation computer would be expensive and would tax its throughput and memory capabilities. Instead, the rotated model coefficients are used to update the nonrotated model coefficients. This is accomplished with the nonrotated model update program which utilizes a Kalman filter. The final state error covariance matrix from the nonrotated model calibration becomes the initial covariance matrix $P$ for the update. The final state error covariance matrix from the rotated model calibration is the measurement noise matrix $R$ for the update. The transformation matrix from the nonrotated model coefficients to the rotated model coefficients (Eq. 5 or 7) is the measurement matrix $M$, and the rotated model coefficients are the measurement vector $Y$. The Kalman equations for the nonrotated model update $X$ are

$$X=KY \tag{17}$$

and

$$K=PM^T(MPM^T+R)^{-1} \tag{18}$$

The update is partitioned into four parts, with the nonrotated angle readout model update and the nonrotated drift rate model update for each ESG being carried out independently.

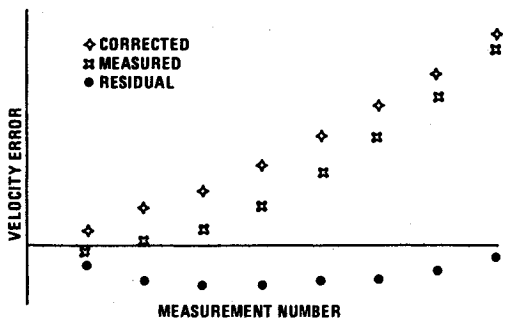


**Fig. 5 Example of measured, corrected, and residual velocity errors for one orientation.**

## Results

N73 high-accuracy calibration data has been taken and processed to obtain rotated model coefficients. These have been used to update the nonrotated model coefficients which were subsequently entered into the N73 navigation computer. Several navigation runs have been performed with the high-accuracy calibration coefficients. In the process of analyzing the results, the nonrotated model has been validated.

Table 1 presents the angle readout coefficients obtained with a high-accuracy calibration. From the angle readout coefficients, it can be seen that the system had angle readout errors of the order of 100 $\mu$rad prior to high-accuracy calibration.

Table 2 presents the drift rate coefficients obtained with a high-accuracy calibration. From the drift rate coefficients, it can be seen that the system had a non-$g$-sensitive drift rate error of the order of 0.01 deg/h prior to high accuracy

**Table 1 Rotated angle readout model coefficients obtained from high-accuracy calibration**

| Gyro | Function | Coefficient, $\mu$rad |
|---|---|---|
| 1 | $P_{1t}$ | 114 |
| 1 | $P_{2t}$ | 7 |
| 1 | $P_{3t}$ | 34 |
| 1 | $P_{4t}$ | −15 |
| 1 | $P_{1c}$ | −36 |
| 1 | $P_{2c}$ | 91 |
| 1 | $P_{3c}$ | −35 |
| 1 | $P_{4c}$ | 1 |
| 2 | $P_{1t}$ | 26 |
| 2 | $P_{2t}$ | −3 |
| 2 | $P_{3t}$ | 41 |
| 2 | $P_{4t}$ | −18 |
| 2 | $P_{1c}$ | 28 |
| 2 | $P_{2c}$ | 66 |
| 2 | $P_{3c}$ | 16 |
| 2 | $P_{4c}$ | −9 |

**Table 2 Rotated drift rate model coefficients obtained with high-accuracy calibration**

| Gyro | Function | Coefficient, deg/h |
|---|---|---|
| 1 | $Q_{1t}$ | 0.0015 |
| 1 | $Q_{2t}$ | −0.0040 |
| 1 | $Q_{4t}$ | 0.0006 |
| 1 | $Q_{1c}$ | −0.0053 |
| 1 | $Q_{2c}$ | −0.0034 |
| 1 | $Q_{4c}$ | −0.0032 |
| 1 | $E_4$ | −0.0068 |
| 1 | $E_{11}$ | 0.0018 |
| 1 | $E_{24}$ | 0.0010 |
| 1 | $E_{32}$ | 0.0021 |
| 1 | $E_{33}$ | −0.0306 |
| 1 | $E_{34}$ | −0.0404 |
| 1 | $E_{35}$ | −0.0049 |
| 2 | $Q_{1t}$ | −0.0024 |
| 2 | $Q_{2t}$ | 0.0016 |
| 2 | $Q_{4t}$ | −0.0005 |
| 2 | $Q_{1c}$ | −0.0088 |
| 2 | $Q_{2c}$ | −0.0063 |
| 2 | $Q_{4c}$ | −0.0018 |
| 2 | $E_4$ | 0.0047 |
| 2 | $E_{11}$ | −0.0076 |
| 2 | $E_{24}$ | 0.0045 |
| 2 | $E_{32}$ | 0.0061 |
| 2 | $E_{33}$ | −0.0104 |
| 2 | $E_{34}$ | 0.0046 |
| 2 | $E_{35}$ | 0.0204 |

**Table 3 Comparison of system performance with and without high-accuracy calibration – laboratory test**

| Date | System no. | Parameters | Comments | Radial error rate, n.mi./h | Rms velocity error, ft/s |
|---|---|---|---|---|---|
| 1-12-78 | 2 | First level | Fast reaction | 0.33 | 0.55 |
| 1-11-78 | 2 | First level | System warm | 0.26 | 0.60 |
| 1-10-78 | 2 | High accuracy | Fast reaction | 0.11 | 0.40 |
| 1-10-78 | 2 | High accuracy | System warm | 0.08 | 0.38 |
| 2-10-78 | 1 | High accuracy | System warm | 0.09 | 0.31 |
| 2-11-78 | 1 | High accuracy | System warm | 0.05 | 0.28 |

**Table 4 Flight test results**

| Date | System no. | Med/high acc soft | Flight route | Flight time, h | Nav time, h | Radial rate, n.mi./h |
|---|---|---|---|---|---|---|
| 9-29-77 | 2 | Med | Saint Louis to Terre Haute to Saint Louis | 2.9 | 3.2 | 0.67 |
| 9-29-77 | 2 | Med | Saint Louis to Terre Haute to Saint Louis | 2.5 | 3.4 | 1.00 |
| 9-30-77 | 2 | Med | Saint Louis to Davenport to Saint Louis | 2.7 | 3.0 | 0.85 |
| 1-27-78 | 2 | High | Saint Louis to Terre Haute to Saint Louis | 2.4 | 2.9 | 0.11 |
| 2-3-78 | 1 | High | Saint Louis to Amarillo | 4.3 | 4.9 | 0.24 |
| 2-4-78 | 1 | High | Amarillo to Burbank | 5.7 | 6.0 | 0.41 |
| 2-4-78 | 1 | High | Burbank to El Paso | 4.6 | 4.8 | 0.33 |

Approximate CEP rate estimates: medium accuracy – three flights, 0.85 n.mi./h
high accuracy – four flights, 0.285 n.mi./h

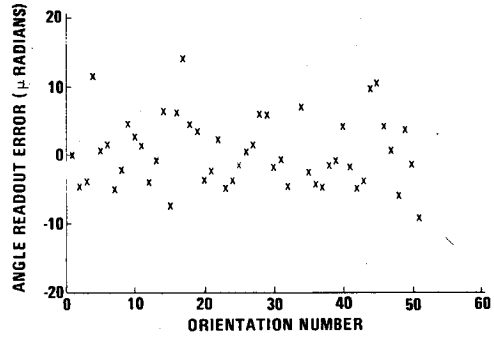


**Fig. 6 Residual angle readout error about north.**

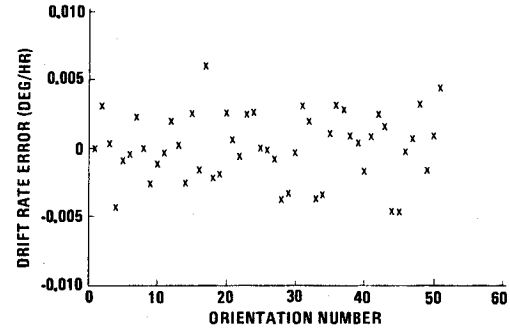


**Fig. 7 Residual drift rate error about north.**

calibration. Some of the $g$-sensitive drift rate coefficients are larger than 0.01 deg/h per $g$ or $g^2$. However, these terms propagate weakly into navigation errors.

Recalling that the nonrotated drift rate function space does not map into the fourth track harmonic of the rotated function space, we note that the coefficients of this harmonic are less than or equal to .0006 deg/h for both ESG's. This is within $2\sigma$ of the estimate error for this harmonic and is within the calibration accuracy goal of .001 deg/h. This lends credence to the high-accuracy calibration methodology, since it says that there are either no significant unmodeled rotated drift rate error terms or, if there are any, their net effect is orthogonal to the fourth track harmonic. It can also be used as a valuable check of calibration and hardware adequacy each time a high-accuracy calibration is performed.

Figures 6 and 7 present the high-accuracy angle readout and drift rate residuals, respectively, about north. These are plotted as a function of the orientation number. The rms residual angle readout and drift rate errors are 5.2 $\mu$rad and 0.0024 deg/h, respectively.

Several laboratory navigation runs have been performed with N73 systems which had high-accuracy calibrations. The results of these runs in terms of CEP are presented in Table 3. The runs each lasted 2 h. The system was pitched 10 deg about east at 40 min and 20 deg about east at 80 min. For comparison purposes, laboratory navigation results are presented for the same system without high-accuracy calibration parameters. The median radial error rate for the laboratory nav runs with and without a high-accuracy calibration was 0.08 n.mi./h and 0.295 n.mi./h, respectively. This represents an accuracy improvement factor of 3.7 to 1.

The N73 strapdown navigator has been flight-tested in cooperation with MDAC, St. Louis. The results are presented in Table 4. For the first three flights, the N73 did not have the benefit of a high-accuracy calibration. The N73 did have a high accuracy calibration for the other four flights. The median radial error rate for the flight tests with and without a high-accuracy calibration was 0.285 n.mi./h and 0.85 n.mi./h, respectively. This represents an improvement factor of 3 to 1. From Tables 3 and 4 it can be seen that the N73 strapdown navigator had significantly higher navigation accuracy when it had a high-accuracy calibration.

## References

[1] Duncan, R.R., "Micron – A Strapdown Inertial Navigator Using Miniature Gyros," Institute of Navigation Conference, March 13-15, 1973.

[2] Schwarz, J.A., "Micro-Navigator (MICRON)," AGARD XXXth Technical Meeting of the Avionic Panel, Sept. 8-12, 1975.

[3] "Micro-Navigator (MICRON) Phase 1A Final Report," Vol. IV, AFAL-TR-72-182, July 1972.

[4] Carlson, N.A., "Fast Triangular Formulation of the Square-Root Filter," *AIAA Journal*, Vol. 11, Sept. 1973, pp. 1259-1265.

[5] Choe, C.Y. and Tapley, B.D., "New Method for Propagating the Square Root Covariance Matrix in Triangular Form," *AIAA Journal*, Vol. 13, May 1975, pp. 681-683.

[6] Gelb, A. (ed.), *Applied Optimal Estimation*, MIT Press, Cambridge, Mass., Feb. 1977.